Journal of Rock Mechanics and Geotechnical Engineering 16 (2024) 1425–1435

Contents lists available at ScienceDirect

Journal of Rock Mechanics and Geotechnical Engineering

journal homepage: www.jrmge.cn

Full Length Article

At-rest lateral earth pressure of compacted expansive soils: Experimental investigations and prediction approach

Zhong Han [a,b,c], Pan Zhang [c], Weilie Zou [a,b,*], Kewei Fan [d,**], Sai K. Vanapalli [c], Lianglong Wan [e]

[a] School of Civil Engineering, Wuhan University, Wuhan, China
[b] Key Laboratory of Rock Mechanics in Hydraulic Structural Engineering of the Ministry of Education, Wuhan University, Wuhan, China
[c] Department of Civil Engineering, University of Ottawa, Ottawa, Ontario, Canada
[d] Key Laboratory of Ministry of Education for Geomechanics and Embankment Engineering, Hohai University, Nanjing, China
[e] Residence Engineering Management Station of Shenzhen Municipality, Shenzhen, China

ARTICLE INFO

Article history:
Received 14 February 2023
Received in revised form
16 August 2023
Accepted 19 October 2023
Available online 17 January 2024

Keywords:
Lateral earth pressure
Expansive soil
Soaking
Vertical stress
Swelling pressure

ABSTRACT

This paper presents experimental studies on a compacted expansive soil, from Nanyang, China for investigating the at-rest lateral earth pressure σ_L of expansive soils. The key studies include (i) relationships between the σ_L and the vertical stress σ_V during soaking and consolidation, (ii) the influences of initial dry density ρ_{d0} and moisture content w_0 on the vertical and lateral swelling pressures at no swelling strain (i.e. σ_{V0} and σ_{L0}), and (iii) evolution of the σ_L during five long-term wetting-drying cycles. Experimental results demonstrated that the post-soaking σ_L-σ_V relationships are piecewise linear and their slopes in the passive state ($\sigma_L > \sigma_V$) and active state ($\sigma_L < \sigma_V$) are similar to that of the consolidation σ_L-σ_V relationships in the normal- and over-consolidated states, respectively. The soaking σ_L-σ_V relationships converge to the consolidation σ_L-σ_V relationships at a threshold σ_V where the interparticle swelling is restrained. The σ_{L0} and σ_{V0} increase monotonically with ρ_{d0}; however, they show increasing-then-decreasing trends with the w_0. The extent of compaction-induced swelling anisotropy, which is evaluated by σ_{L0}/σ_{V0}, reduces with an increase in the compaction energy and molding water content. The σ_L reduces over moisture cycles and the stress relaxation in the σ_L during soaking is observed. An approach was developed to predict the at-rest soaking σ_L-σ_V relationships, which requires conventional consolidation and shear strength properties and one measurement of the σ_L-σ_V relationships during soaking. The proposed approach was validated using the results of three different expansive soils available in the literature.

1. Introduction

Expansive soils exhibit remarkable swelling upon wetting in both vertical and lateral directions. When the lateral swelling is restrained by adjacent structures (e.g. retaining walls, bridge piers, tunnel linings), reaction stress develops and imposes extra thrust on these structures in addition to the conventional lateral earth pressure. Experimental investigations and field observations have revealed that the lateral earth pressure on retaining structures in expansive soils could be several times the conventional lateral earth pressure (Katti et al., 1983; Sorochan and Ryabova, 1988; Fourie, 1989; Wang et al., 2008; Avsar et al., 2009; Mohamed et al., 2014; Saba et al., 2014; Sun et al., 2014; Yuan et al., 2016; Al-Juari et al., 2021), which leads to the distress and failure (Pufahl et al., 1983; Chen, 1988; Zheng et al., 2009; Nelson et al., 2015; Liu and Vanapalli, 2017; Yao et al., 2020; Zhang et al., 2020a). Therefore, the reliable determination and estimation of the lateral earth pressure of expansive soils are essential in the rational design of geotechnical structures in expansive soil regions.

The lateral earth pressure of expansive soils (denoted as σ_L) during wetting under the at-rest condition (i.e. laterally swelling is strictly restrained, also known as the K_0 condition) is frequently investigated as it is easy to measure and represents the worst-case scenario for retaining structures (Kate and Katti, 1983; Abbas et al., 2015; Wan et al., 2018; Niu et al., 2020; Zhang et al., 2020a).

* Corresponding author. School of Civil Engineering, Wuhan University, Wuhan, China
** Corresponding author.
E-mail addresses: zwilliam@whu.edu.cn (W. Zou), kw_fan@hhu.edu.cn (K. Fan).
Peer review under responsibility of Institute of Rock and Soil Mechanics, Chinese Academy of Sciences.

https://doi.org/10.1016/j.jrmge.2023.10.014

Oedometer-style devices are frequently used to measure the at-rest σ_L of small-scale expansive soil specimens. Equipment such as stress sensors (Pincus et al., 1993; Ikizler et al., 2008; Saba et al., 2013, 2014; Rawat et al., 2019; Zhang et al., 2020a), sealed hydraulic or air chambers with pore-pressure sensors (Monroy et al., 2015; Puppala et al., 2016; Wan et al., 2018) and piston device with reaction force measurements (Katti, 1979; Kate and Katti, 1983) can be affixed to or integrated with the sidewall of the oedometer-style devices to facilitate the direct measurement of the σ_L. Alternatively, some researches measure the hoop strain of the laterally pressurized thin-wall oedometer rings using strain gauges and calibrate the strain readings towards the applied lateral stress. The strain readings are then used to determine the at-rest σ_L of expansive soil specimens during inundation (Ofer, 1981; Avsar et al., 2009; Abbas et al., 2015; Pirjalili et al., 2020).

Conventional triaxial cells (Fourie, 1989; Boyd and Sivakumar, 2011) and three-dimensional (3D) swelling devices (Zhang, 1990; Sun et al., 2013; Saba et al., 2014; Chi et al., 2018) have also been used for σ_L measurements. The advantage of these devices is that they can be used to track the variation of the σ_L during the alleviation of lateral restraint (Al-Shamrani, 2004; Chi et al., 2018; Zhang et al., 2020b). In addition, large-scale model tests (Katti et al., 1983; Wang et al., 2008; Al-Juari et al., 2021; Fan et al., 2023) and in situ tests and observations (Kassiff and Zeitlen, 1961; Clayton et al., 1991; Brackley and Sanders, 1992; Mohamed et al., 2014) on the development of σ_L during infiltration are reported in the literature. Comprehensive summaries of existing techniques for measuring the σ_L of expansive soils are available in Liu and Vanapalli (2019).

The σ_L is sensitive to various factors including (i) mineralogy and pore-fluid chemistry (Tripathy et al., 2014; Por et al., 2017; Chen et al., 2022), (ii) physical states such as void ratio, dry density, moisture content, and fabric (Sun et al., 2013; Sivakumar et al., 2015; Wang et al., 2021), and (iii) stress and strain constraints such as internal soil suction, external stress and strain boundary conditions (Kate and Katti, 1983; Boyd and Sivakumar, 2011; Niu et al., 2020; Pirjalili et al., 2020; Zhang et al., 2020a; Liu et al., 2021; Selçuk, 2022). For expansive soils with specific chemical and physical indices, the variation of the σ_L with the vertical stress σ_V is the key information in the design of retaining structures for determining the lateral loads considering the surcharge and embedment depth of expansive soils.

The at-rest σ_L-σ_V relationships of expansive soils upon infiltration are non-linear, state-dependent, and are influenced by the anisotropy of the expansive soil (Kate and Katti, 1983; Avsar et al., 2009; Abbas et al., 2015; Zhang et al., 2020a). There are several empirical approaches in the literature to estimate the σ_L from the σ_V (Hong, 2008; Wang et al., 2008; Nelson et al., 2015). The limitation of these approaches is that their validity is limited for certain soil types and testing conditions. Alternatively, semi-empirical and theoretical approaches based on the constitutive relationships were also developed for expansive soils (Liu and Vanapalli, 2017, 2019; Abdollahi and Vahedifard, 2021). Such approaches are versatile and capable of accounting for various influencing factors. However, they require a considerable amount of testing data and careful calibration of model parameters. For this reason, they may not be viable for small-scale projects or preliminary designs. Hence, simple yet reliable approaches for estimating the σ_L are still desirable in engineering practice. Besides, surficial expansive soils behind retaining structures are typically subjected to drying-wetting cycles during the service life. The influence of long-term moisture cycling on the σ_L and the time dependency of the σ_L are important aspects in the design practice but are less investigated in the literature.

This paper presents a series of experimental studies on the at-rest lateral earth pressure of a compacted expansive soil upon soaking. The influences of vertical stress, compaction moisture content, and density, compaction-induced residual lateral stress, and long-term drying-wetting cycles on the at-rest σ_L were studied. Based on the experimental results, a simple approach is proposed in this paper to estimate the correlations between the at-rest lateral earth pressure and the vertical stress. The performance of the proposed approach was further validated using the experimental data of three expansive soils reported in the literature.

2. Experimental investigations

2.1. Material and equipment

The expansive soil investigated in this study was a brownish-yellow surficial soil collected from Nanyang in Henan Province, China (referred to as Nanyang expansive soil). Expansive soils in Nanyang are typically alluvial deposits and diluvium formed during the mid-Pleistocene epoch. Their parent rocks are granite, marlstone, and claystone. They are distributed close to the ground surface and typically extend 15–40 m in thickness (Feng et al., 2005). Nanyang expansive soils exhibit medium to high swelling potential and have reportedly induced numerous engineering problems and hazards to the associated geo-structures, especially the canal slopes and retaining structures of China's South-to-North Water Transfer Project that passes through the Nanyang district (Zhao et al., 2015; Zhang et al., 2016). The moisture content and dry density of the excavated soil samples were 13%–21% and 1200–1800 kg/m^3, respectively.

The collected soil samples were air-dried, pulverized, and passed through a sieve with 2 mm openings for subsequent experimental investigations. X-ray diffraction (XRD) tests were performed to determine the mineralogy of the Nanyang expansive soil (see Fig. 1). The matrix flushing approach was adopted to determine the contents of the major minerals, which are 25% (by mass) for the montmorillonite, 5% for the illite, 5% for the kaolinite, 44% for the quartz, 17% for the albite, and 2% for the calcite.

Table 1 summarizes the material properties of the Nanyang expansive soil. This soil exhibits (i) medium swelling potential based on its free swell ratio $\delta_{ef} = 70\%$, as per the Chinese National Technical Code for Buildings in Expansive Soil Regions (GB50112-2013, 2013) (low: $40 \leq \delta_{ef} < 65$, medium: $65 \leq \delta_{ef} < 90$, high: $\delta_{ef} \geq 90$) or (ii) very high swelling potential based on its plasticity index, I_P and clay fraction, according to Van der Merwe (1964). The

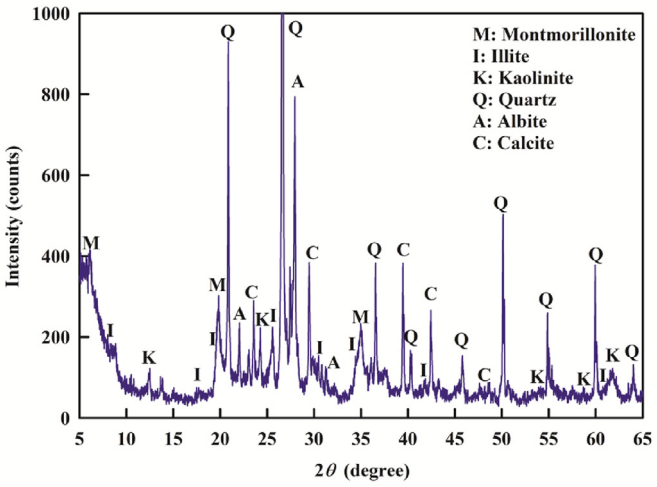

Fig. 1. XRD results of the Nanyang expansive soil.

Table 1
Material properties of expansive soils investigated in this study.

Property	Value			
	Nanyang expansive soil	Al-Qatif clay	Baise expansive soil	Black cotton soil
Specific gravity, G_s	2.71	2.74	2.75	2.78
Sand-size particles (%)	10		0	12
Silt-size particles (%)	54		52	32
Clay-size particles (%)	36	~42	48	56
Plastic limit, w_P (%)	23	60	21	43
Liquid limit, w_L (%)	66	140	56	82
Plasticity index, I_P	43	80	35	39
USCS classification[a]	CH	CH	CH	CH-MH
Free-swell ratio, δ_{ef} (%)	70		82	~100
Swelling potential per δ_{ef}[b]	Medium		Medium	High
Swelling potential per I_P and clay fraction[c]	Very high	Very high	High	Very high
Source	This study	Abbas et al. (2015)	Zhang et al. (2020a)	Kate and Katti (1983)

[a] ASTM D2487-11 (2011).
[b] GB50112-2013 (2013).
[c] Van der Merwe (1964).

optimum moisture content w_{opt} and maximum dry density ρ_{dmax} of the Nanyang expansive soil, which were determined from standard Proctor tests per the ASTM D698 standard (ASTM D698-12, 2012), are 16.7% and 1820 kg/m^3, respectively.

A modified oedometer (Fig. 2) was used to measure the σ_L. This oedometer incorporates a water chamber that is in contact with the specimen's shaft through a rubber ring. The rubber ring is made of elastic rubber which is highly flexible. The water chamber is filled with de-aired water and sealed by valves. After the installation of specimens, small water pressure (about 2–3 kPa) is applied such that the rubber slightly expands and becomes in close contact with the specimens. Since the sealed de-aired water is incompressible, this system guarantees the at-rest condition of the specimen during swelling or consolidation and measures its σ_L through the pore-pressure sensor (capacity = 1 MPa, accuracy = 0.2 kPa). The axial load is applied by the loading cap and the vertical displacement can be registered using digital dialgage to determine the variation in the specimen's void ratio e, and axial strain ε_a. Details of this oedometer including verification of its at-rest condition and accuracy of measurements are available in Wan et al. (2018).

2.2. Specimens preparation and testing procedures

Three different types of tests were performed: (i) soaking-consolidation tests under designated vertical stress to investigate the σ_L-σ_V relationships after soaking and during the subsequent consolidation; (ii) constant volume soaking tests to study the influences of compaction dry density (ρ_{d0}) and compaction moisture content (w_0) on the σ_L, and (iii) long-term wetting-drying tests to reveal the variation of σ_L during long-term cyclic moisture variation. The specimens used for all the tests were 61.8 mm in diameter and 20 mm in height. Dry soil was thoroughly mixed with water to achieve designated w_0 values. The moist soil was statically compacted in oedometer rings or the modified oedometer (inner diameter = 61.8 mm, inner height = 20 mm) to the designed ρ_{d0} to form the specimens. The ρ_{d0} was achieved by controlling the mass and volume of the compacted soil.

2.2.1. Soaking-consolidation tests

Specimens were compacted at a w_0 of 17% and a ρ_{d0} of 1500 kg/m^3, which corresponds to the average in situ moisture-density condition of the excavated soil samples. Their initial void ratio e_0 was 0.806. A total of 12 parallel specimens were compacted. They were divided into six pairs. In each pair, one specimen was directly compacted in the modified oedometer (the inner dimension of the specimen chamber is 61.8 mm in diameter and 20 mm in height). Valves of the de-aired water chamber were closed during the compaction to preserve the compaction-induced residual lateral stress, σ_{res}. The other specimen was compacted in an oedometer ring with the same inner dimension as the modified oedometer. It was retrieved from the ring after compaction and installed into the oedometer, during which the valves of the water chamber remained open. After installation of the specimen, the de-aired water in the water chamber was slightly pressurized to 5 kPa to ensure good contact between the rubber ring and the specimens. The valves were closed thereafter. This procedure eliminates the σ_{res} (Tripathy et al., 2014). Consequently, the comparison between the results of the paired specimens reveals the influence of σ_{res} on the development of σ_L of expansive soils.

After the compaction or installation of specimens in the modified oedometer, six levels of vertical stress (σ_V = 1, 12.5, 25, 50, 100, and 200 kPa) were applied to the six pairs of specimens, respectively (i.e. specimens in each pair were subjected to the same σ_V). It took about 1 d for the vertical deformation (i.e. swelling or compression) of specimens to stabilize (i.e. vertical deformation <0.04 mm, swelling or compression strain <0.2% per day). Thereafter, the σ_V was maintained while soaking started. Water was introduced to saturate the specimen through the top and bottom

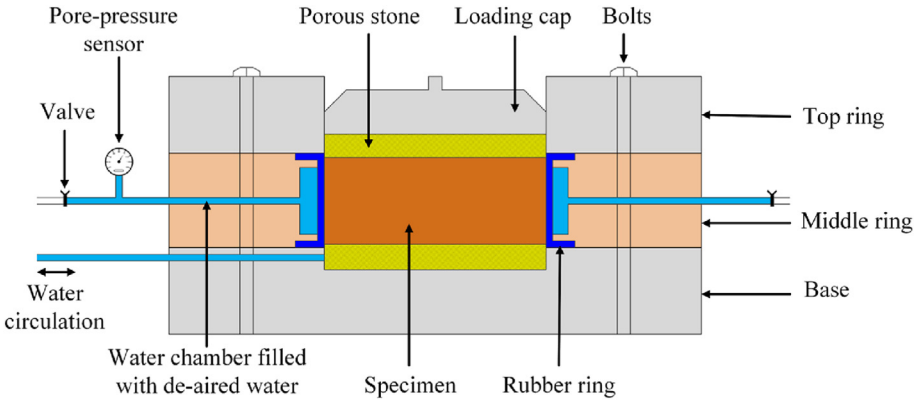

Fig. 2. Modified oedometer for measuring the lateral earth pressure.

porous stones (see Fig. 2). Saturated status in the specimen was deemed achieved once the variation in the vertical deformation and σ_L had stabilized (i.e. vertical deformation <0.04 mm, swelling or compression strain <0.2%, and $\Delta\sigma_L < 1$ kPa per day). It generally took about 2–3 d for the soaking process to complete. After soaking, consolidation tests followed, during which the σ_V was increased in steps to about 250 kPa. The variation of the σ_L and vertical strain of the specimens with time and σ_V was measured during the entire testing procedure.

2.2.2. Constant volume soaking tests

Two groups of specimens were tested. In the first group, all specimens were compacted at a constant w_0 of 17% but five different ρ_{d0} values (i.e. 1300, 1400, 1500, 1600, and 1700 kg/m^3). Specimens in the second group were compacted at a constant ρ_{d0} of 1500 kg/m^3 but five different w_0 values (i.e. 12%, 17%, 22%, 27%, 30%). These varying ρ_{d0} and w_0 values were chosen referencing the range of the moisture-density conditions of the excavated soil samples. Specimens were compacted in oedometer rings and thereafter retrieved from the rings and transferred to the modified oedometer.

During the constant volume soaking tests, a low initial σ_V was first applied to the specimens before soaking. After water is introduced, the specimen starts to swell and the σ_V was increased to suppress the development of swelling strain. The σ_V was continuously adjusted in this manner until the specimens ceased to swell (Zhang et al., 2020; Zhang and Cui, 2022). The final stabilized vertical stress, σ_{V0}, and lateral earth pressure, σ_{L0} (conventionally referred to as vertical swelling pressure and lateral swelling pressure, respectively) were recorded.

2.2.3. Long-term wetting-drying tests

The specimen was compacted at a w_0 of 17% and a ρ_{d0} of 1500 kg/m^3 ($e_0 = 0.806$) in an oedometer ring before being transferred into the modified oedometer. It was subjected to five consecutively conducted wetting (i.e. soaking) and drying processes under a constant σ_V of 50 kPa. In each cycle, the soaking process lasted about 20 d, which is much longer than the soaking duration in the soaking-consolidation and constant volume soaking and tests. The prolonged soaking period is adopted to observe the evolution of the σ_L with time for saturated specimens.

During drying, the specimen was left in the oedometer to slowly evaporate at room temperature. The drying process ended when the height of specimens ceased to decrease. The first drying process took about 30 d while the following drying processes took about 20 d. The variation of the σ_L and ε_a with time t during the five wetting-drying cycles, which took more than 200 d, were recorded.

3. Interpretation of experimental results

3.1. Influence of compaction-induced residual lateral stress on lateral earth pressure

The development of the σ_L with t during the application of σ_V (at $t = 0$) and the subsequent soaking process in the soaking-consolidation tests is shown in Fig. 3 for specimens with and without σ_{res} under three σ_V levels. For specimens without σ_{res}, the measured σ_L upon the application of σ_V before soaking is the lateral earth pressure of the unsaturated specimens due to surcharge. The σ_L is minimal under low σ_V and only approaches 10 kPa when σ_V rises to 200 kPa. The initial σ_L of specimens with σ_{res} is in the range of 60–80 kPa and consists of the σ_{res} and the lateral earth pressure due to surcharge. Evident stress relaxation can be observed before soaking.

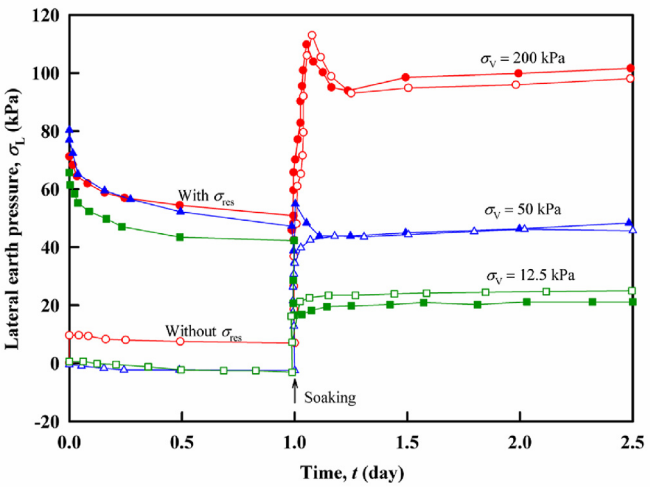

Fig. 3. Influence of σ_{res} on the development of σ_L.

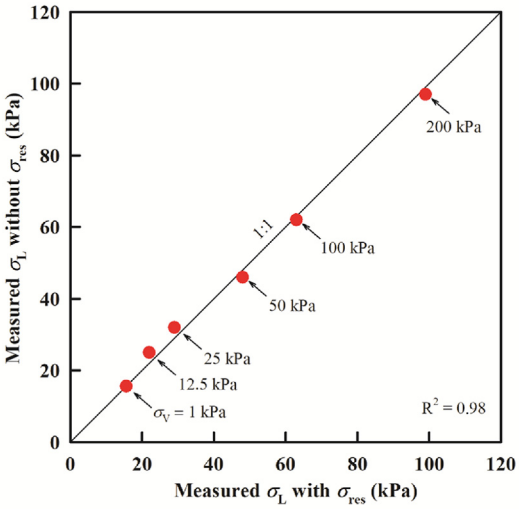

Fig. 4. Comparisons between σ_L of specimens with and without σ_{res} after soaking.

The σ_L changes drastically upon soaking and stabilizes after about 1 d. Upon soaking, the σ_L of specimens without σ_{res} increases under all σ_V levels while the σ_L of specimens with σ_{res} adjusts accordingly to be consistent with the stabilized σ_L of specimens without σ_{res}. In other words, the influence of the σ_{res} on the σ_L is eliminated during soaking. Similar to the results of the σ_L, the development of vertical strain with time for specimens with and without σ_{res} is consistent under different σ_V levels. In other words, specimens after soaking have similar void ratios regardless of the σ_{res}. This indicates that the σ_{res} has no influence on the volumetric behavior of the tested expansive soil under K_0 condition.

For the variation of σ_L during soaking under high σ_V of 200 kPa particularly, an evident increase-decrease trend can be observed from specimens with and without σ_{res}. Similar observations were also reported in the literature (Windal and Shahrour, 2002; Boyd and Sivakumar, 2011; Abbas et al., 2015) and attributed to the "wetting collapse" of unsaturated soils (i.e. soil yields under constant σ_V during wetting) (Boyd and Sivakumar, 2011; Han et al., 2019) and the yielding due to the reverse of major principal stresses when σ_L exceeds σ_V (Brown and Sivakumar, 2008).

To better capture and understand such behaviors, the development of lateral stress with suction and moisture content, as well as the soil water characteristics of unsaturated expansive soil specimens during wetting, is required (Monroy et al., 2015; Pasha et al., 2016). Due to the limitation of the testing equipment in this study for controlling or measuring the soil suction and moisture content, such behaviors of unsaturated specimens during wetting are not discussed in this paper.

Fig. 4 shows comparisons between the measured σ_L from specimens with and without σ_{res} under all σ_V levels. No noticeable differences can be observed and the coefficient of determination (R^2) for the two groups of measurements is 0.98. Results shown in Figs. 3 and 4 indicate that the σ_{res} does not impact the at-rest σ_L of soaked specimens. This is consistent with results reported by Tripathy et al. (2014) for a compacted bentonite that the σ_L after soaking is not sensitive to the σ_{res} when $\sigma_L < 3000$ kPa. Due to these reasons and for simplicity, specimens without σ_{res} were used for further tests and analyses.

3.2. Void ratio-vertical stress-lateral earth pressure relationships after soaking and during consolidation

The variations in e and σ_L of the specimens with σ_V during soaking and the subsequent consolidation processes are shown in Fig. 5. After soaking, specimens swell remarkably under a nominal σ_V of 1 kPa (marked point O). With increasing σ_V, the global volumetric swelling gradually reduces and finally transfers to collapse. The e decreases from 0.806 to 0.72 at $\sigma_V = 200$ kPa (marked point B). The boundary delimitating the swelling and collapse behaviors is close to $\sigma_V = 100$ kPa where e remains approximately constant after soaking (see Fig. 5a). This is corroborated by the results of constant volume soaking tests performed on identical specimens which give $\sigma_{V0} = 89$ kPa and $\sigma_{L0} = 58$ kPa at a constant e of 0.806 (this point is also shown in Fig. 5 and marked as point D).

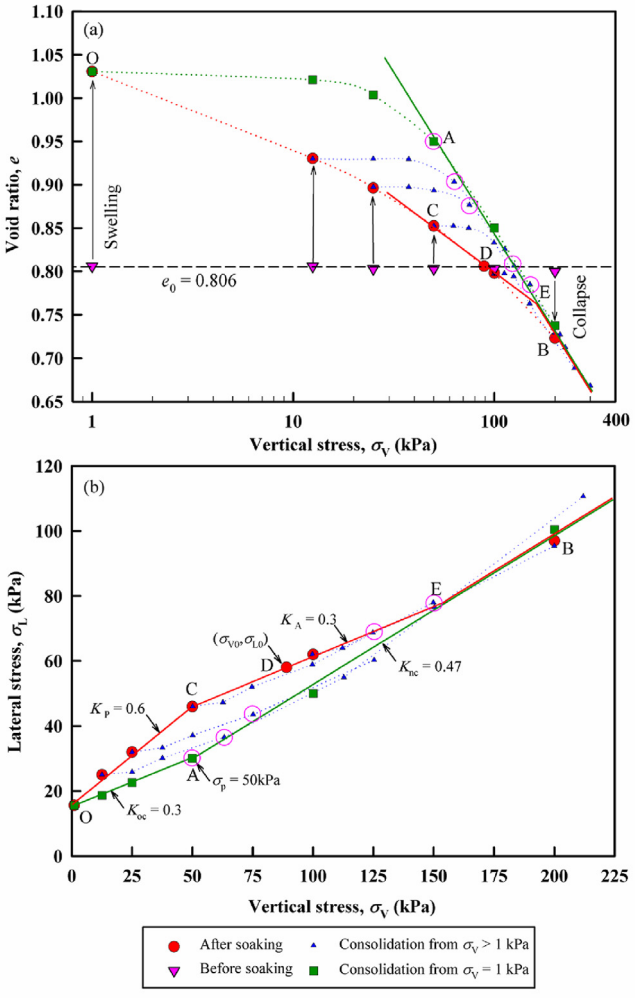

Fig. 5. (a) e-σ_V and (b) σ_L-σ_V relationships after soaking and during consolidation.

The e-σ_V relationships of the saturated specimens after soaking (referred to as soaking e-σ_V relationships) and during the subsequent consolidation (referred to as consolidation e-σ_V relationships) show hysteretic characteristics when $\sigma_V \leq 100$ kPa. At $\sigma_V = 200$ kPa and beyond, these two e-σ_V relationships become identical. All consolidation e-σ_V curves, regardless of the applied σ_V during soaking, converge to a unique normal consolidation line upon yielding (i.e. when σ_V exceeds the pre-consolidation stress, σ_p). All yielding points for the e-σ_V and σ_L-σ_V relationships during consolidation are circled in Fig. 5.

The normal consolidation line is indicated by line AB where point A is the yielding point of the specimen soaked under $\sigma_V = 1$ kPa ($\sigma_p = 50$ kPa). Line AB registers a $\sigma_V = 125$ kPa at $e = e_0 = 0.806$ (the corresponding $\sigma_L = 70$ kPa). The σ_V and σ_L obtained from such swelling-consolidation-to-e_0 procedure are 40% and 21% higher than the σ_{V0} and σ_{L0} obtained from constant volume soaking tests, respectively. This confirms that the swelling-then-consolidation-to-e_0 procedure overestimates the vertical as well as the lateral swelling pressures (Yang et al., 2014; Liu and Vanapalli, 2017).

The σ_L-σ_V relationships after soaking (referred to as soaking σ_L-σ_V relationships) and during consolidation (referred to as consolidation σ_L-σ_V relationships) are hysteretic and piece-wise linear (see Fig. 5b). All consolidation σ_L-σ_V relationships (e.g. broken line $OAEB$ for the specimen consolidated under $\sigma_V = 1$ kPa) turn at their σ_p (highlighted with circles in Fig. 5b). In the over-consolidated state where $\sigma_V < \sigma_p$, the consolidation σ_L-σ_V relationships are parallel and have a uniform slope of 0.3 (denoted the earth pressure coefficient for over-consolidated soils, K_{oc}). The consolidation σ_L-σ_V relationships in the normal-consolidated state where $\sigma_V > \sigma_p$ converge to line AB with a slope of 0.47 (denoted the earth pressure coefficient for normal-consolidated soils, K_{nc}). These observations are consistent with behaviors of non-swelling saturated soils (Mesri and Hayat, 1993) and indicate that the K_{oc} and K_{nc} are insensitive to the σ_V applied during soaking.

The soaking σ_L-σ_V relationships (i.e. broken line $OCEB$ in Fig. 5b) can be divided into three sections: OC, CE, and EB. In section OC, specimens stay in a passive stress state where $\sigma_L > \sigma_V$. The slope of line OC, denoted K_P, is 0.6. Point C ($\sigma_V = 50$ kPa $\approx \sigma_L = 46$ kPa) indicates the reversal of the principal stresses, beyond which specimens are in an active stress state ($\sigma_L < \sigma_V$) and their σ_L-σ_V relationships stay on line CE. Point D (σ_{V0}, σ_{L0}) also stays on line CE. The slope of line CE, denoted K_A, is 0.3. Line CE intersects the normal-consolidation σ_L-σ_V relationships (line AB) at point E ($\sigma_V = 154$ kPa, $\sigma_L = 78$ kPa), beyond which the soaking σ_L-σ_V relationships (line EB) converge to the normal-consolidation σ_L-σ_V relationships (line AB). Point E on the e-σ_V plot (see Fig. 5a) also marks the merge of the soaking e-σ_V curve to the consolidation e-σ_V curve.

The experimental results shown in Fig. 5 deserve discussion from following two aspects.

(i) Variation of swelling pressure and swelling potential with external stress

The hysteresis in the soaking and consolidation σ_L-σ_V relationships (between point *O* and point *E* in Fig. 5b) indicates the existence of the lateral pressure induced purely due to swelling, σ_S. The measured σ_L after soaking comprises of the σ_S and the conventional lateral earth pressure, σ_E (i.e. $\sigma_L = \sigma_S + \sigma_E$) (Liu and Vanapalli, 2017; Zhang et al., 2020a). Under the same σ_V, the gap between the soaking and consolidation σ_L-σ_V relationships is a measurement of the σ_S. With an increase in the σ_V, the two σ_L-σ_V lines become closer, meaning that the σ_S reduces with an increase in the external stress. If σ_S is used to scale the swelling potential of expansive soils, the complete restraint of the lateral swelling potential takes place at point *E* where $\sigma_S = 0$. This is reflected in the σ_L-σ_V and *e*-σ_V relationships that beyond point *E*, the hysteresis ceases and the soaking σ_L-σ_V relationships completely converge to the consolidation σ_L-σ_V relationships.

The σ_V and σ_L at point *E* are significantly larger than the σ_{V0} and σ_{L0} at point *D* where hysteresis and σ_S still exist (see Fig. 5b). This means that simply arresting the swelling strain is not enough to eliminate the swelling pressure and restrain the swelling potential. Upon soaking under a certain σ_V, the global volumetric behavior of expansive soils results from the competition between (i) the swelling of the clay matrix caused by the thickening of the double-layer and (ii) the compression of the soil skeleton under external stress. Nil global volumetric strain indicates that the swelling is entirely offset by the compression. This, however, does not guarantee the cease of the inter-particle swelling since the σ_S still exists. With further increase in the σ_V, although global compression is demonstrated, the clay matrix may still swell and occupy the macro-pore space in the soil skeleton until a threshold σ_V at point *E* is achieved.

(ii) Similarities between the soaking and consolidation σ_L-σ_V relationships

In the active zone, the soaking σ_L-σ_V relationships *CE* is parallel to or overlapped with the over-consolidation σ_L-σ_V relationships *OA* ($K_A = K_{oc} = 0.3$). The soaking σ_L-σ_V relationships *OC* in the passive zone is seemingly different from that in the active zone but approximately parallel to the normal-consolidation σ_L-σ_V relationships *AB* ($K_P \approx K_{nc}$). A phenomenological deduction is thus established that the expansive soil after soaking stays in an elastic state in the active zone just like the over-consolidated soil and elastoplastic state in the passive zone similar to the soil during the normal consolidation.

Zhang et al. (2018) reported that the at-rest σ_L-σ_V relationships obtained from a single specimen soaked under a high σ_V and subsequently unloaded are similar to the soaking σ_L-σ_V relationships formed by results of individual specimens soaked under different values of σ_V. If soaking σ_L-σ_V relationships are comparable to the unloading σ_L-σ_V relationships, the initial unloading from high σ_V in the active zone would be elastic, and further unloading in the passive zone would be elastoplastic due to the reversal of principal stresses, and the associated passive shearing. This illustration matches the phenomenological deduction for the soaking σ_L-σ_V relationships.

Based on these observations, it appears that the slope of the σ_L-σ_V relationships for the tested expansive soil in the elastic state is unique regardless of the stress and hydration histories (i.e. $K_A = K_{oc}$). However, the slopes of the soaking and consolidation σ_L-σ_V relationships in the elastoplastic state, although close (i.e. $K_P \approx K_{nc}$), are different due to the differences in the direction of principal stresses and direction of shearing, and the influence of anisotropy.

The stress state after soaking and during consolidation are shown on the *q*-*p* plot in Fig. 6 where deviator stress $q = \sigma_V - \sigma_L$ and mean stress $p = (\sigma_V + 2\sigma_L)/3$. Soil behavior is elastic in zone *OAEC* which is bounded by two extremes of elastic behavior (i.e. *OA* and *CE*, which correspond to the elastic σ_L-σ_V relationships) and two yielding planes (i.e. *AB* and *OC*, which correspond to the elasto-plastic σ_L-σ_V relationships).

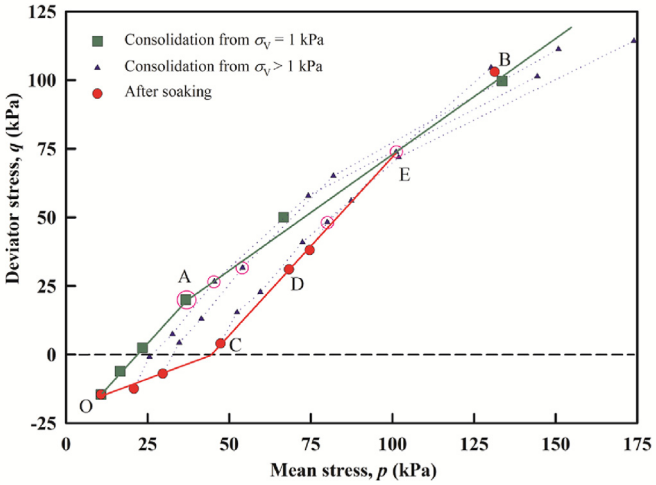

Fig. 6. *q*-*p* relationships after soaking and during consolidation.

3.3. Influences of compaction density and moisture content on the lateral and vertical swelling pressures

The variations of the σ_{V0} and σ_{L0} that were obtained from constant volume soaking tests and their ratio (σ_{L0}/σ_{V0}) with the compaction dry density ρ_{d0} are shown in Fig. 7. It should be noted that although the σ_{L0} is conventionally termed as the lateral swelling pressure, it consists not only the lateral pressure merely induced by swelling σ_S but also the conventional lateral earth pressure σ_E associated with the vertical stress σ_{V0}.

The σ_{L0} and σ_{V0} increase with ρ_{d0} and the $\log_{10}\sigma_{L0}$-ρ_{d0} and $\log_{10}\sigma_{V0}$-ρ_{d0} relationships are linear and can be fitted by simple linear equations (see Fig. 7). These observations are expected and consistent with results of similar experimental studies in the literature (Qin et al., 2009; Sun et al., 2013; Chi et al., 2018; Zou et al., 2020). Greater density means more hydrophilic clay particles and larger specific area within a unit volume of expansive soil,

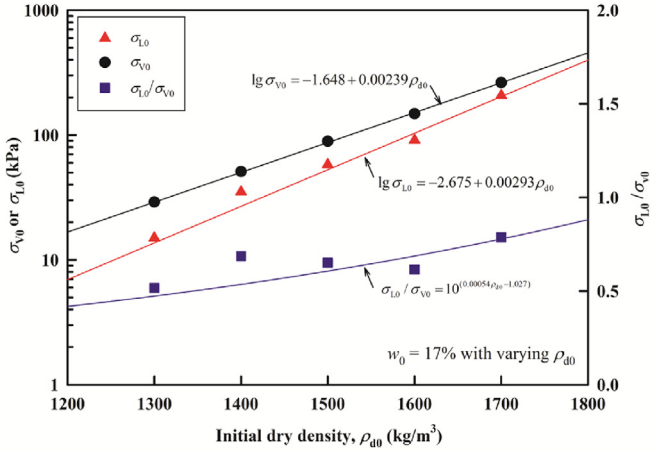

Fig. 7. Variation of σ_{V0} and σ_{L0} and their ratio with the ρ_{d0}.

which results in greater swelling potential and swelling pressure upon soaking.

The ratio of σ_{L0}/σ_{V0} slightly increases as the ρ_{d0} increases, which is consistent with the results of similar experimental studies (e.g. Chi et al., 2018). The σ_{L0}/σ_{V0} versus ρ_{d0} relationship can be described using a power function derived from the linear $\log_{10}\sigma_{L0}$-ρ_{d0} and $\log_{10}\sigma_{V0}$-ρ_{d0} relationships, as shown in Fig. 7. The density-dependency of the σ_{L0}/σ_{V0} can be attributed to the amount of lateral and vertical voids inside the soil. During the one-dimensional compaction, lateral voids, the orientation of which is perpendicular to the direction of compaction, are first compressed under low compaction energy. The vertical voids, whose orientation is parallel to the direction of compaction, are generally compressed after lateral voids under higher compaction energy. There are more vertical voids in specimens with low ρ_{d0} than in specimens with high ρ_{d0} since denser specimens require higher compaction energy to compress vertical voids. Upon swelling, vertical voids can accommodate the swelling of clay minerals and contribute to alleviating the development of lateral swelling pressure. Consequently, the development of lateral swelling pressure of looser specimens with more vertical voids is less significant compared with that of denser specimens with fewer vertical voids, which results in the behavior that the σ_{L0}/σ_{V0} increases with the ρ_{d0}.

Fig. 8 summarizes the variation of the σ_{L0}, σ_{V0}, and their ratio σ_{L0}/σ_{V0} with the compaction water content w_0. The σ_{L0} and σ_{V0} initially increase with the w_0, peak at $w_0 = 22\%$, and reduce with further increase in the w_0. Such behaviors are possibly the results of the interplay of the following two factors.

Clayey soils typically demonstrate aggregated structure with distinct aggregate-clay matrix dual structure characteristics when compacted at low w_0. The degree of aggregation of clay particles increases with the w_0. As the w_0 further increases beyond certain thresholds (typically the optimum moisture content, which is 16.7% for the tested soil), the soil structure gradually transfers to a dispersed fashion within which the clay aggregates become less notable and the soil texture becomes homogenous (Vanapalli et al., 1999; Leroueil and Hight, 2013; Han and Vanapalli, 2016; Han et al., 2022; Pei et al., 2024). The aggregated structure is more stable upon loading and exhibits higher stiffness and strength properties compared to the dispersed structure. Due to this reason, its reaction stress during confined soaking (i.e. σ_{L0}, σ_{V0}) will be higher.

At a constant ρ_{d0}, the increase in the w_0 leads to an increase in the degree of particle hydration and a reduction in the volume of air-filled voids of the compacted specimens. Consequently, the amount of water absorbed during the confined soaking reduces, which further results in the reduction in the swelling potential and σ_{L0} and σ_{V0}.

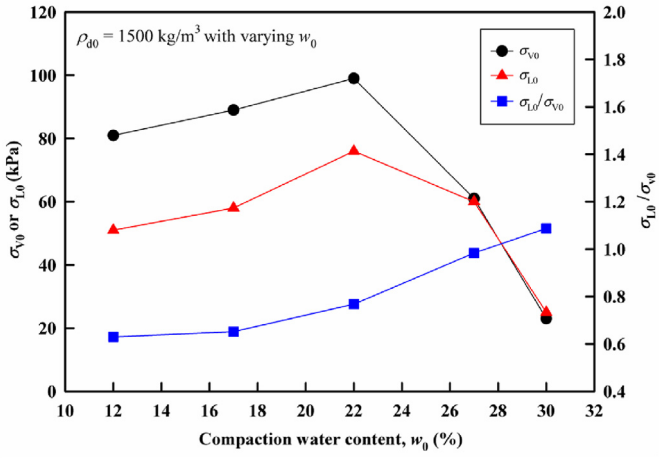

Fig. 8. Variation of σ_{V0} and σ_{L0} with w_0.

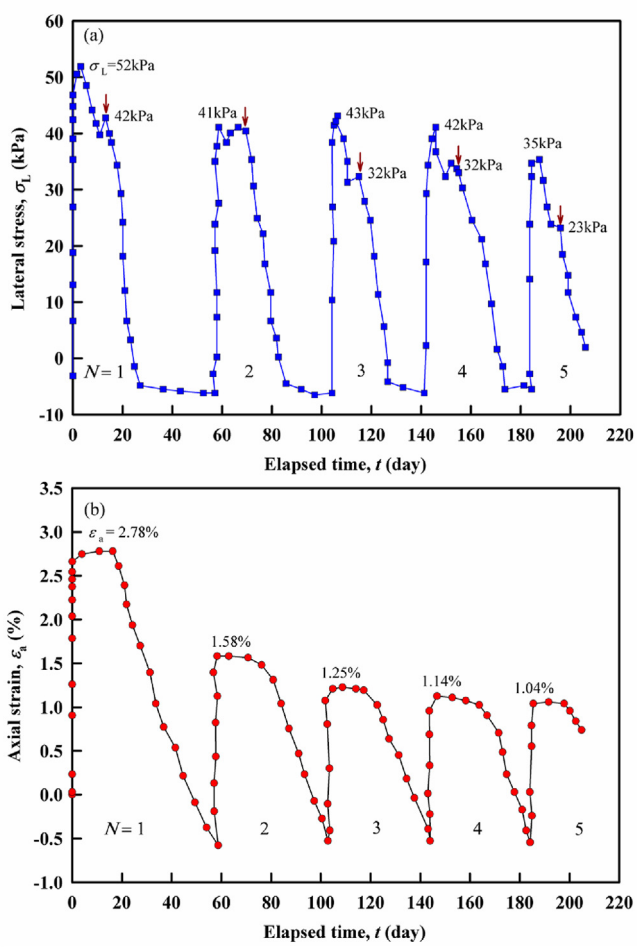

Fig. 9. Evolution of (a) σ_L and (b) ε_a during long-term moisture cycles.

Regardless of the parabolic swelling pressure-w_0 relationships, the σ_{L0}/σ_{V0} increases monotonically from 0.65 at $w_0 = 12\%$ to 1.1 at $w_0 = 30\%$, which indicates that the degree of compaction-induced swelling anisotropy reduces with increasing w_0 under the constant volume soaking condition. At $w_0 = 30\%$, specimens after compaction were approximately saturated. Still, σ_{L0} and σ_{V0} of about 20 kPa were measured upon soaking. This confirms that apparent saturated expansive soils continue to absorb water and develop swelling pressure upon soaking (Tu and Vanapalli, 2016).

3.4. Evolution of lateral earth pressure during long-term moisture cycles

The evolutions of the σ_L and ε_a during five long-term drying and wetting cycles under a σ_V of 50 kPa are shown in Fig. 9. The following can be observed:

(1) The σ_L upon soaking reduces during moisture cycles and the reduction is most significant during the first cycle. The peak σ_L right after soaking reduces from the initial value of 52 kPa–41 kPa after one cycle (reduction of 21%) and 35 kPa after four cycles (reduction of 33%).

(2) Stress relaxation takes place during the soaking process that lasts about 20 d in almost every moisture cycle. The reduction in the σ_L due to stress relaxation is about 10–12 kPa. The extent of stress relaxation increases with moisture cycles. For example, during the first soaking process, the σ_L reduces from 52 kPa immediately after soaking to 42 kPa at the end of soaking (marked by arrows), constituting a relaxation ratio of 19%. In the fifth cycle, σ_L reduces from 35 kPa to 23 kPa and the relaxation ratio is 34%.

(3) The ε_a upon soaking also reduces during moisture cycles and the reduction is most significant after the first cycle. This is consistent with similar experimental results reported in the literature (Alonso et al., 2005; Tripathy and Subba Rao, 2009; Estabragh et al., 2015). On the other hand, the ε_a after drying is not affected by moisture cycling and stays at about −0.5% during the cycles.

(4) The σ_L drops quickly when drying starts, which is associated with the lateral shrinkage of the specimens during drying. The σ_L drops to 0 during every drying process, indicating that specimens detach from the rubber membrane. In the subsequent drying process, the specimens continue to shrink in all directions, as can be judged from the continuous development in the axial strain (see Fig. 9). It should be noted that such shrinkage is no longer under the K_0 condition but the 3D condition.

The reductions in the σ_L and ε_a, and the increase in the stress relaxation are associated with the weakening of the soil skeleton due to the presence of wetting-drying-induced microscopic and macroscopic fissures, especially for expansive soils (Zhao et al., 2021; Han et al., 2022). In fact, visible cracks (i.e. macroscopic fissures) were observed on the surface of the specimens after the long-term wetting-drying tests. The swelling potential and the resistance to lateral stress reduce when the soil skeleton is weakened.

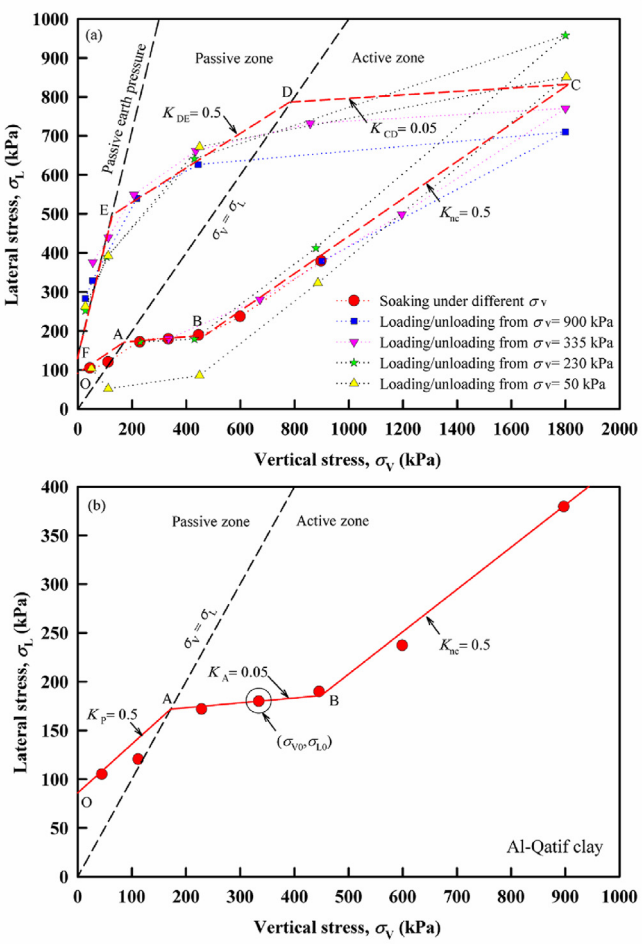

Fig. 11. The σ_L-σ_V relationships of the Al-Qatif clay: (a) Measurements during soaking-loading-unloading, and (b) Measurements versus predictions.

4. Approach for estimating the lateral earth pressure

4.1. Development of the approach

An approach is developed to estimate the at-rest σ_L-σ_V relationships for compacted expansive soils upon soaking based on experimental observations obtained in this study. The estimated σ_L-σ_V relationships are confined by two boundaries and are linear in the active zone ($\sigma_L < \sigma_V$) and the passive zone ($\sigma_L > \sigma_V$), as shown in Fig. 10.

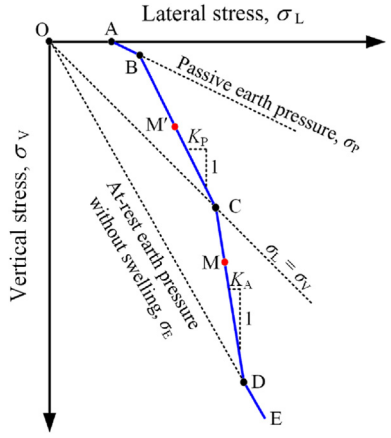

Fig. 10. The proposed approach for estimating the soaking σ_L-σ_V relationships.

The upper boundary of the at-rest σ_L-σ_V relationships is the passive earth pressure σ_P of the saturated expansive soils (Pufahl et al., 1983; Liu and Vanapalli, 2017), which can be determined following conventional passive earth pressure theories using the effective cohesion c' and effective friction angle ϕ' of the soils (line *AB* in Fig. 10). Passive shear failure usually takes place close to the ground surface where σ_V is low. Surficial expansive soils are typically subjected to moisture and temperature cycles that significantly reduce the shear strength of the soils (Han et al., 2022; Zou et al., 2022). Determination of the c' and ϕ' of surficial expansive soils considering weathering effects is thus important for the rational determination of this upper boundary. Only expansive soils that develop large σ_L under low σ_V may experience passive shear failure. The soaking σ_L-σ_V relationships of expansive soils with low or medium swelling potentials (such as the Nanyang expansive soil) usually fall below this passive failure envelope.

According to the experimental results from this study (see Fig. 5), the at-rest σ_L-σ_V relationships in the passive zone (line *BC* in Fig. 10) and active zone (line *CD* in Fig. 10) are linear and their slopes (K_P and K_A) are comparable to the conventional earth pressure coefficients (K_{nc} and K_{oc}). For simplification purposes, this study assumes $K_P = K_{nc}$ and $K_A = K_{oc}$. With the further increase in the σ_V in the active zone, the soaking σ_L-σ_V relationships converge to the consolidation σ_L-σ_V relationships at point *D*.

To locate the piece-wise σ_L-σ_V relationships *ABCDE*, one measurement of the σ_L-σ_V relationship either in the active zone (i.e. point *M*) or passive zone (i.e. point *M′*) is necessary. This measurement could be the σ_L-σ_V relationships frequently measured for design practice such as the swelling pressures at no swelling strain (σ_{L0}, σ_{V0}) or the σ_L under a certain σ_V level (usually 50 kPa in practice). With this one measurement and conventional earth pressure and shear strength data (i.e. K_{nc}, K_{oc}, c' and ϕ'), one can easily establish the entire at-rest σ_L-σ_V relationships upon soaking.

In addition, empirical correlations can be used for estimating the K_{nc} and K_{oc}, and thus K_P and K_A (Eqs. (1) and (2)) (Jaky, 1944; Mesri and Hayat, 1993) if this information is not available (e.g. during preliminary design or design for new soils without existing experience). However, due to their empirical nature, Eqs. (1) and (2) cannot guarantee accurate estimations of K_{nc} and K_{oc} for all soils. Thus, they should be used with caution.

$$K_P = K_{nc} = 1 - \sin\phi' \tag{1}$$

$$K_A = K_{oc} = 0.75(1 - \sin\phi') \tag{2}$$

4.2. Validation of the proposed approach

Experimental data obtained from three different expansive soils, namely Al-Qatif clay from Turkey (Abbas et al., 2015), Baise expansive soil from China (Zhang et al., 2020a), and black cotton soil from India (Kate and Katti, 1983) are used to validate the proposed approach. The basic soil properties of these soils are summarized in Table 1.

4.2.1. Validation using results of Al-Qatif clay

Abbas et al. (2015) investigated the σ_L-σ_V relationships of the compacted Al-Qatif clay using a thin-walled oedometer. Parallel specimens (w_0 = 31.1%–31.9%, ρ_{d0} = 1201 kg/m^3) were first soaked under σ_V ranging from 50 to 900 kPa, then incrementally loaded to a σ_V of 1800 kPa, and finally step-wisely unloaded to a σ_V of 25 kPa. The (σ_{L0}, σ_{V0}) at no swelling strain was also measured. Fig. 11a presents the measured σ_L-σ_V relationships.

The σ_L-σ_V relationships after soaking and during the subsequent consolidation show that: (i) the soaking σ_L-σ_V relationships are piecewise linear and turn at $\sigma_L = \sigma_V$ (point A) and a threshold σ_V of about 450 kPa (point *B*); (ii) all post-soaking consolidation σ_L-σ_V relationships, along with the soaking σ_L-σ_V relationships, converge to a unique normal-consolidation σ_L-σ_V relationship (line *BC*) when σ_V exceeds 450 kPa. These observations are consistent with the experimental results of the Nanyang expansive soil and validate the key assumptions used to develop the approach for estimating the soaking σ_L-σ_V relationships. It is noted that the σ_L measured at σ_V = 1800 kPa is scattered and ranges between 700 kPa and 950 kPa. This is possible because the thin-walled oedometer used by Abbas et al. (2015) was only calibrated to a maximum σ_L of about 800 kPa. The average value of the measured σ_L (i.e. σ_L = 800 kPa) was used to locate point *C*, which, however, agrees well with the trends of the measurements.

The unloading σ_L-σ_V relationships also show piecewise linear trends in the active zone (line *CD*) and passive zone (line *DE*). At the end of unloading ($\sigma_V < 200$ kPa), apparent passive shear failure can be observed (line *EF*). The initial unloading in the active zone is elastic and its slope K_{CD} equals the soil's K_{oc} (i.e. $K_{CD} = K_{oc} = 0.05$) (Mesri and Hayat, 1993). Unloading in the passive zone is elasto-plastic and per the previous analysis in this paper, its slope K_{DE} should be similar to the soil's K_{nc}. As a matter of fact, line *DE* is indeed parallel to the normal-consolidation σ_L-σ_V line *BC* in Fig. 11 (i.e. $K_{DE} = K_{nc} = 0.5$).

Following the approach proposed in this paper, the slopes of the soaking σ_L-σ_V relationships are determined, $K_P = K_{nc} = 0.5$, $K_A = K_{oc} = 0.05$. The measured (σ_{L0}, σ_{V0}) of the Al-Qatif clay is used as the required one measurement of the σ_L-σ_V relationship. Fig. 11b shows the measured (in symbols) and predicted (in lines) soaking σ_L-σ_V relationships. Good agreement can be observed between the measurements and predictions.

4.2.2. Validation using results of baise expansive soil and black cotton soil

Zhang et al. (2020a) investigated the soaking σ_L-σ_V relationships of the Baise expansive soil using a modified oedometer that measures the σ_L through a pressure sensor mounted on the side of the oedometer ring. Specimens were compacted at the same ρ_{d0} of 1602 kg/m^3 but three w_0 levels (i.e. 17.9%, 20.3%, and 22.5%). Kate and Katti (1983) evaluated the soaking σ_L-σ_V relationships of the black cotton soil using a cylindrical container with a piston device mounted on the shaft for σ_L measurements. Specimens were compacted at ρ_{d0} = 1418 ± 10 kg/m^3 and w_0 = 9 ± 1%.

The consolidation data K_{nc} and K_{oc} values of these two soils are not available in their original studies. Zhang et al. (2020a) reported c' = 12 kPa and ϕ' = 32° for the Baise expansive soil, and Katti (1979) reported c' = 25 kPa and ϕ' = 25° for the black cotton soil compacted in a manner similar to that adopted by Kate and Katti (1983). The c' and ϕ' values are used to establish Rankine's passive earth pressure envelope and estimate the K_P and K_A using Eqs. (1) and (2), respectively. The (σ_{L0}, σ_{V0}) of the two soils are used as the required one measurement of the σ_L-σ_V relationship.

Figs. 12 and 13 provide comparisons between the measured soaking σ_L-σ_V relationships (symbols) and the corresponding predictions using the proposed approach (continuous lines). Both soils demonstrate bi-linear σ_L-σ_V relationships in the active and passive zones, which is reasonably described by the proposed approach. The predictions also capture the passive shear failure of the black cotton soil, as shown in Fig. 13. There are certain deviations between the measurements and predictions for the Baise expansive soil, as shown in Fig. 12. This is possibly related to the uncertainties in the estimated the K_A and K_P from Eqs. (1) and (2). Using actual K_{nc} and K_{oc} values (i.e. K_A and K_P values) derived from consolidation tests might result in better predictions.

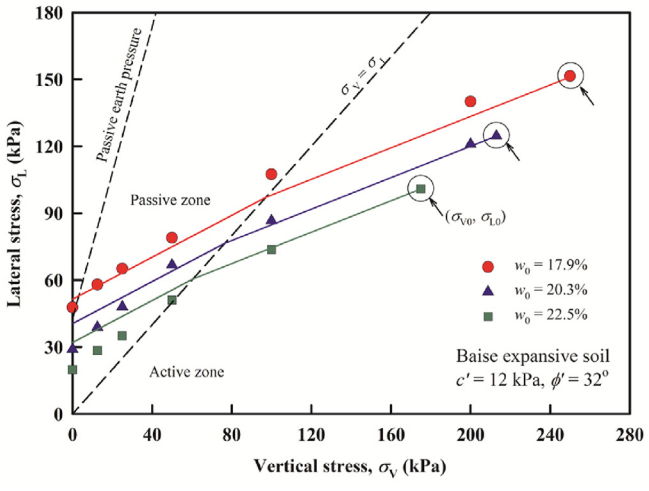

Fig. 12. Measured and predicted σ_L-σ_V relationships of the Baise expansive soil.

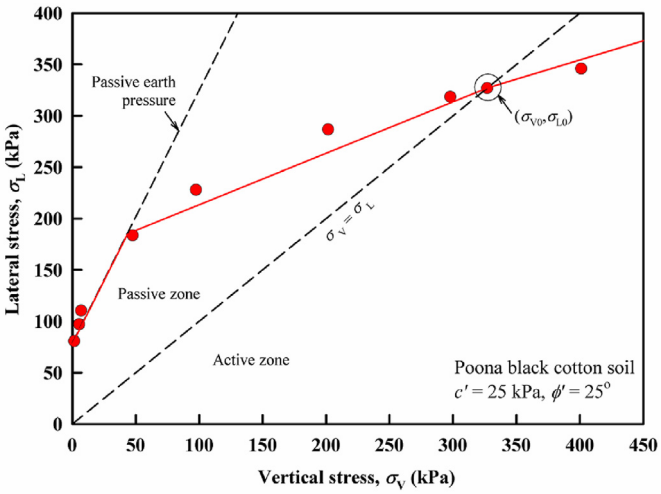

Fig. 13. Measured and predicted soaking σ_L-σ_V relationships of the black cotton soil.

5. Conclusions

The at-rest lateral earth pressure σ_L of a compacted expansive soil upon soaking was studied. The influences of several key factors, including the vertical stress σ_V, residual lateral stress during compaction σ_{res}, compaction dry density ρ_{d0}, and moisture content w_0, were evaluated. The evolution of the σ_L during long-term wetting-drying cycles that lasted over 200 d was also determined. Experimental results have revealed that:

(1) The σ_{res} does not impose significant influences on the σ_L upon soaking. The at-rest σ_L-σ_V relationships upon soaking are piecewise linear in the passive zone ($\sigma_L > \sigma_V$) and active zone ($\sigma_L < \sigma_V$). Their slopes K_P and K_A are related to that of the conventional consolidation σ_L-σ_V relationships K_{nc} and K_{oc} (i.e. $K_P \approx K_{nc}$ and $K_A = K_{oc}$). Expansive soils after soaking possibly stay in an elastic state in the active zone and an elastoplastic state in the passive zone.

(2) The soaking σ_L-σ_V relationships converge to the consolidation σ_L-σ_V relationships at a threshold σ_V beyond which the interparticle swelling ceases. The lateral pressure induced purely due to swelling, σ_S still exists when the global volumetric swelling strain is completely restrained or even when the soil shows collapse behavior upon soaking. The σ_S reduces to zero at the threshold σ_V.

(3) The swelling pressures σ_{L0} and σ_{V0} at no swelling strain increase with ρ_{d0} and the $\log_{10}\sigma_{L0}$-ρ_{d0} and $\log_{10}\sigma_{V0}$-ρ_{d0} relationships are linear. The σ_{L0} and σ_{V0} show increase-then-decrease variations with the w_0 which peak at $w_0 = 22\%$. The ratio σ_{L0}/σ_{V0} increases with both ρ_{d0} and w_0, indicating that the extent of compaction-induced swelling anisotropy reduces with increasing compaction energy and molding water content.

(4) The σ_L remarkably reduces over long-term wetting-drying cycles and the reduction is most significant after the first cycle. Stress relaxation in the σ_L takes place during soaking and its extent increases with wetting-drying cycles.

Based on the obtained experimental observations, an approach was developed to estimate the at-rest soaking σ_L-σ_V relationships for expansive soils. This approach is simple and only requires one measurement of the soaking σ_L-σ_V relationships and conventional consolidation and shear strength properties for prediction. The approach is examined using the results of three different expansive soils reported in the literature. It is demonstrated that the proposed approach is capable of suitably capturing the piecewise linear and passive shear failure characteristics of the soaking σ_L-σ_V relationships of expansive soils.

Declaration of competing interest

The authors declare that they have no known competing financial interests or personal relationships that could have appeared to influence the work reported in this paper.

Acknowledgments

Studies presented in this paper were sponsored by the National Natural Science Foundation of China (Grant Nos. 52378365 and 52179109), Jiangsu Province Excellent Postdoctoral Program (Grant No. 2023), and China Scholarship Council-University of Ottawa Joint Scholarship.

References

Abbas, M.F., Elkady, T.Y., Al-Shamrani, M.A., 2015. Evaluation of strain and stress states of a compacted highly expansive soil using a thin-walled oedometer. Eng. Geol. 193, 132–145.
Abdollahi, M., Vahedifard, F., 2021. Model for lateral swelling pressure in unsaturated expansive soils. J. Geotech. Geoenviron. Eng. 147, 04021096.
Al-Juari, K.A.K.K., Fattah, M.Y., Khattab, S.I.A.A., Al-Shamam, M.K., 2021. Simulation of behaviour of swelling soil supported by a retaining wall. Proc. Inst. Civ. Eng. - Struct. Build. 175, 1–10.
Al-Shamrani, M.A., 2004. Influence of lateral restraint on the swelling behavior of expansive soils. J. Southeast Asian Geotech. Soc. 101–111.
Alonso, E.E., Romero, E., Hoffmann, C., García-Escudero, E., 2005. Expansive bentonite–sand mixtures in cyclic controlled-suction drying and wetting. Eng. Geol. 81, 213–226.
ASTM D698-12, 2012. Standard Test Methods for Laboratory Compaction Characteristics of Soil Using Standard Effort (12400 Ft-Lbf/ft3 (600 kN-M/m3)). ASTM International, West Conshohocken, PA, USA.
ASTM D2487-11, 2011. Standard Practice for Classification of Soils for Engineering Purposes (Unified Soil Classification System). ASTM International, West Conshohocken, PA, USA.
Avsar, E., Ulusay, R., Sonmez, H., 2009. Assessments of swelling anisotropy of Ankara clay. Eng. Geol. 105, 24–31.
Boyd, J.L., Sivakumar, V., 2011. Experimental observations of the stress regime in unsaturated compacted clay when laterally confined. Geotechnique 61, 345–363.
Brackley, I.J.A., Sanders, P.J., 1992. In situ measurement of total natural horizontal stresses in an expansive clay. Geotechnique 42, 443–451.
Brown, J.L., Sivakumar, V., 2008. The Change in Stress Regime during Wetting of Unsaturated Compacted Clays when Laterally Confined. Proc. 1st Eur. Conf. E-UNSAT, Durham, United Kingdom, pp. 361–367.
Chen, F.H., 1988. Foundations on Expansive Soils. Elsevier, New York, USA.
Chen, Y.G., Cai, Y.Q., Pan, K., Ye, W.M., Wang, Q., 2022. Influence of dry density and water salinity on the swelling pressure and hydraulic conductivity of compacted GMZ01 bentonite–sand mixtures. Acta Geotech 17, 1879–1896.
Chi, Z.C., Chen, S.X., Dai, Z.J., Zhou, Z., Song, R., 2018. Research on strain regularity of three-dimensional stress of Hefei remolded expansive clay. Chin. J. Rock Mech. Eng. 37, 3359–3365 (in Chinese).
Clayton, C.R.I., Symons, I.F., Hiedra-Cobo, J.C., 1991. The pressure of clay backfill against retaining structures. Can. Geotech. J. 28, 282–297.
Estabragh, A.R., Parsaei, B., Javadi, A.A., 2015. Laboratory investigation of the effect of cyclic wetting and drying on the behaviour of an expansive soil. Soils Found. 55, 304–314.
Fan, K., Yang, G., Zou, W., Han, Z., Shen, Y., 2023. Lateral earth pressure of granular backfills on retaining walls with expanded polystyrene geofoam inclusions under limited surcharge loading. J. Rock Mech. Geotech. Eng. https://doi.org/10.1016/j.jrmge.2023.11.005.
Feng, Y.Y., Xu, W.Y., Wang, S.J., Qu, Y.X., 2005. Engineering geological characteristics and suitability for embankment of Nanyang expansive soils. Rock Soil Mech. 26, 1645–1651.
Fourie, A.B., 1989. Laboratory evaluation of lateral swelling pressure. J. Geotech. Eng. 115, 1481–1486.
GB50112-2013, 2013. Technical Code for Buildings in Expansive Soil Regions. China Architecture and Building Press, Beijing.
Han, Z., Vanapalli, S.K., 2016. Stiffness and shear strength of unsaturated soils in relation to soil-water characteristic curve. Geotechnique 66, 627–647.
Han, Z., Vanapalli, S.K., Zou, W., Wang, X., Zhang, J., 2019. Modelling virgin compression line of compacted unsaturated soils. Acta Geotech 14, 1991–2006.

Han, Z., Zhao, G., Lin, J., Fan, K., Zou, W., 2022. Influences of temperature and moisture histories on the hydrostructural characteristics of a clay during desiccation. Eng. Geol. 297, 106533.
Hong, G.T., 2008. Earth Pressures and Deformations in Civil Infrastructure in Expansive Soils. PhD Thesis. Texas A&M University, Texas, USA.
Ikizler, S.B., Aytekin, M., Nas, E., 2008. Laboratory study of expanded polystyrene (EPS) geofoam used with expansive soils. Geotext. Geomembranes 26, 189–195.
Jaky, J., 1944. The coefficient of earth pressure at rest. J. Hungarian Soc. Archit. Eng. 78, 355–358.
Kassiff, G., Zeitlen, J.G., 1961. Lateral Swelling Pressure on Conduits from Expansive Clay Backfill. 40th Annu. Meet. Highw. Res. Board, Washington, D.C, pp. 1–11.
Kate, J.M., Katti, R.K., 1983. Lateral pressures at rest in expansive soil covered with cohesive nonswelling soil. Soils Found. 23, 58–68.
Katti, R.K., 1979. Search for solutions to problems in black cotton soils. Indian Geotech. J. 9, 1–82.
Katti, R.K., Bhangale, E.S., Moza, K.K., 1983. Lateral Pressure in Expansive Soil with and without a Cohesive Non-swelling Soil Layer—Application to Earth Pressures on Cross Drainage Structures in Canals and Key Walls in Dams (Studies on K0 Condition). Central Board of Irrigation and Power, New Delhi, India.
Leroueil, S., Hight, D.W., 2013. Compacted soils: from physics to hydraulic and mechanical behaviour. Adv. Unsaturated Soils. 41–59.
Liu, Y., Vanapalli, S.K., 2019. Prediction of lateral swelling pressure behind retaining structure with expansive soil as backfill. Soils Found. 59, 176–195.
Liu, Y., Vanapalli, S.K., 2017. Influence of lateral swelling pressure on the geotechnical infrastructure in expansive soils. J. Geotech. Geoenviron. Eng. 143, 04017006.
Liu, Z., Zhang, R., Liu, Z., Zhang, Y., 2021. Experimental study on swelling behavior and its anisotropic evaluation of unsaturated expansive soil. Adv. Mater. Sci. Eng. 1–13.
Mesri, G., Hayat, T.M., 1993. The coefficient of earth pressure at rest. Can. Geotech. J. 30, 647–666.
Mohamed, O.Z., Taha, Y.K., El-Aziz, E.M.A., 2014. Field study of the distribution of lateral swelling pressure of expansive soil on retaining structure. J. Eng. Sci. 42, 289–302.
Monroy, R., Zdravkovic, L., Ridley, A.M., 2015. Mechanical behaviour of unsaturated expansive clay under K_0 conditions. Eng. Geol. 197, 112–131.
Nelson, J.D., Chao, K.C., Overton, D.D., Nelson, E.J., 2015. Foundation Engineering for Expansive Soils. Wiley, Hoboken, NJ, USA.
Niu, W.J., Ye, W.M., Song, X., 2020. Unsaturated permeability of Gaomiaozi bentonite under partially free-swelling conditions. Acta Geotech 15, 1095–1124.
Ofer, Z., 1981. Laboratory instrument for measuring lateral soil pressure and swelling pressure. Geotech. Test J. 4, 177.
Pasha, A.Y., Khoshghalb, A., Khalili, N., 2016. Pitfalls in interpretation of gravimetric water content–based soil-water characteristic curve for deformable porous media. Int. J. GeoMech. 16, D4015004.
Pei, Q., Zou, W., Han, Z., Wang, X., Xia, X., 2024. Compression behaviors of a freeze–thaw impacted clay under saturated and unsaturated conditions. Acta Geotech. https://doi.org/10.1007/s11440-023-02188-6.
Pincus, H., Habib, S., Karube, D., 1993. Swelling pressure behavior under controlled suction. Geotech. Test J. 16, 271–275.
Pirjalili, A., Garakani, A.A., Golshani, A., Mirzaii, A., 2020. A suction-controlled ring device to measure the coefficient of lateral soil pressure in unsaturated soils. Geotech. Test J. 43, 20190099.
Por, S., Nishimura, S., Likitlersuang, S., 2017. Deformation characteristics and stress responses of cement-treated expansive clay under confined one-dimensional swelling. Appl. Clay Sci. 146, 316–324.
Pufahl, D.E., Fredlund, D.G., Rahardjo, H., 1983. Lateral earth pressures in expansive clay soils. Can. Geotech. J. 20, 228–241.
Puppala, A.J., Pedarla, A., Hoyos, L.R., Zapata, C., Bheemasetti, T.V., 2016. A semi-empirical swell prediction model formulated from 'clay mineralogy and unsaturated soil' properties. Eng. Geol. 200, 114–121.
Qin, B., Chen, Z., Liu, Y., Wang, J., 2009. Characteristics of 3D swelling pressure of GMZ001 bentonite. Chin. J. Geotech. Eng. 31, 756–763.
Rawat, A., Baille, W., Tripathy, S., 2019. Swelling behavior of compacted bentonite-sand mixture during water infiltration. Eng. Geol. 257, 105141.
Saba, S., Barnichon, J.D., Cui, Y.J., Tang, A.M., Delage, P., 2014. Microstructure and anisotropic swelling behaviour of compacted bentonite/sand mixture. J. Rock Mech. Geotech. Eng. 6, 126–132.
Saba, S., Cui, Y.J., Tang, A.M., Barnichon, J.D., 2013. Investigation of the swelling behaviour of compacted bentonite–sand mixture by mock-up tests. Can. Geotech. J. 51, 1399–1412.
Selçuk, L., 2022. A rational method for determining the swelling pressure of expansive soils: paired swell test (PS-test). Acta Geotech 17, 3161–3180.
Sivakumar, V., Zaini, J., Gallipoli, D., Solan, B., 2015. Wetting of compacted clays under laterally restrained conditions: initial state, overburden pressure and mineralogy. Geotechnique 65, 111–125.
Sorochan, E.A., Ryabova, M.S., 1988. Pressure of swelling soil against retaining walis. Soil Mech. Found. Eng. 25, 101–105.
Sun, D., Sun, W., Fang, L., 2014. Swelling characteristics of Gaomiaozi bentonite and its prediction. J. Rock Mech. Geotech. Eng. 6, 113–118.
Sun, F., Chen, Z., Qin, B., et al., 2013. Characteristics of three-dimensional swelling pressure of Gaomiaozi bentonite-sand mixture. Chin. J. Rock Mech. Eng. 32, 200–207 (in Chinese).
Tripathy, S., Bag, R., Thomas, H.R., 2014. Effects of post-compaction residual lateral stress and electrolyte concentration on swelling pressures of a compacted bentonite. Geotech. Geol. Eng. 32, 749–763.
Tripathy, S., Subba Rao, K.S., 2009. Cyclic swell-shrink behaviour of a compacted expansive soil. Geotech. Geol. Eng. 27, 89–103.
Tu, H., Vanapalli, S.K., 2016. Prediction of the variation of swelling pressure and one-dimensional heave of expansive soils with respect to suction using the soil-water retention curve as a tool. Can. Geotech. J. 53, 1213–1234.
Vanapalli, S.K., Fredlund, D.G., Pufahl, D.E., 1999. The influence of soil structure and stress history on the soil–water characteristics of a compacted till. Geotechnique 49, 143–159.
Van der Merwe, D.H., 1964. The prediction of heave from the plasticity index and percentage clay fraction of soil. Civ. Eng. Soc. Africa. 6, 103–107.
Wan, L., Zou, W., Wang, X., Han, Z., 2018. Comparison of three inclusions in reducing lateral swelling pressure of expansive soils. Geosynth. Int. 25, 481–493.
Wang, D.W., Zhu, C., Tang, C.S., et al., 2021. Effect of sand grain size and boundary condition on the swelling behavior of bentonite–sand mixtures. Acta Geotech 16, 2759–2773.
Wang, N., Zhang, W., Gu, X., Zeng, Y., 2008. Lateral swelling pressure of expansive soil acting on retaining wall due to inundation. J. Hydraul. Eng. 39, 580–587 (in Chinese).
Windal, T., Shahrour, I., 2002. Study of the swelling behavior of a compacted soil using flexible odometer. Mech. Res. Commun. 29, 375–382.
Yang, G.L., Teng, K., Qin, C.H., 2014. An in-situ experimental research of lateral swelling pressure on expansive soils. J. Cent. South Univ. 45, 2326–2332.
Yao, H., She, J., Lu, Z., et al., 2020. Inhibition effect of swelling characteristics of expansive soil using cohesive non-swelling soil layer under unidirectional seepage. J. Rock Mech. Geotech. Eng. 12, 188–196.
Yuan, S., Liu, X., Sloan, S.W., Buzzi, O.P., 2016. Multi-scale characterization of swelling behaviour of compacted Maryland clay. Acta Geotech 11, 789–804.
Zhang, F., Cui, Y., 2022. Microstructure-based insight into different swelling pressure determination methods. Eng. Geol. 307, 106777.
Zhang, F., Cui, Y., Conil, N., Talandier, J., 2020. Assessment of swelling pressure determination methods with intact Callovo-Oxfordian claystone. Rock Mech. Rock Eng. 53, 1879–1888.
Zhang, J., Sun, D., Zhou, A., Jiang, T., 2016. Hydromechanical behaviour of expansive soils with different suctions and suction histories. Can. Geotech. J. 53, 1–13.
Zhang, R., Liu, Z., Zheng, J., Zhang, J., 2020a. Experimental evaluation of lateral swelling pressure of expansive soil fill behind a retaining wall. J. Mater. Civ. Eng. 32, 04019360.
Zhang, R., Zhang, B., Zheng, J., Liu, Z., 2018. Modified lateral confined swelling tests on expansive soils. Chin. J. Geotech. Eng. 40, 2223–2230 (in Chinese).
Zhang, R., Zhao, X., Zheng, J., Liu, Z., 2020b. Experimental study and application of lateral swelling stress of expansive soil. China J. Highw. Transp. 33, 22–31 (in Chinese).
Zhang, Y., 1990. Laboratory investigation of three-dimensional swell-shrinkage characteristics of expansive soils. Dam Obs. Geotech. Tests. 1, 13–22 (in Chinese).
Zhao, G., Han, Z., Zou, W., Wang, X., 2021. Evolution of mechanical behaviours of an expansive soil during drying-wetting, freeze–thaw, and drying-wetting-freeze–thaw cycles. Bull. Eng. Geol. Environ. 80, 8109–8121.
Zhao, H., Liu, J., Guo, J., Zhao, C., Gong, B., 2015. Reexamination of lime stabilization mechanisms of expansive clay. J. Mater. Civ. Eng. 27, 04014108.
Zheng, J., Zhang, R., Yang, H., 2009. Highway subgrade construction in expansive soil areas. J. Mater. Civ. Eng. 21, 154–162.
Zou, W., Han, Z., Ye, J., 2020. Influence of external stress and initial density on the volumetric behavior of an expansive clay during wetting. Environ. Earth Sci. 79, 211.
Zou, W., Han, Z., Zhao, G., Fan, K., Vanapalli, S.K., Wang, X., 2022. Effects of cyclic freezing and thawing on the shear behaviors of an expansive soil under a wide range of stress levels. Environ. Earth Sci. 81, 77.

Zhong Han obtained his BSc and MSc degrees in Geotechnical Engineering from Zhengzhou University, China in 2009 and 2012, respectively, and his PhD in Civil Engineering from the University of Ottawa, Canada in 2016. He is currently affiliated as Associate Professor at the School of Civil Engineering, Wuhan University, China, and Adjunct Professor at the Department of Civil Engineering, University of Ottawa, Canada. His research interests include (i) elastoplastic responses of unsaturated soils upon static, dynamic, and hydraulic loadings; (ii) behaviors of pavement soils (aggregates and subgrade soils) and pavement structure under the influences of external environment (drying-wetting-freeze-thaw actions); and (iii) volumetric and mechanical behaviors expansive soils and associated mitigation approaches. He has authored more than 60 journal publications in either Chinese or English on these research topics and has participated in several research projects funded by the National Natural Science Foundation of China, National Key Research & Development Program of China, and MTO, NSERC, NRC in Canada. More information can be found at http://jszy.whu.edu.cn/hanzhong/zh_CN/index.htm.